











Cite this: DOI: 10.1039/d6sc02258h

All publication charges for this article have been paid for by the Royal Society of Chemistry

# Synthesis, characterization, and imidogen photochemistry of a hydrazoic acid adduct of Rh<sub>2</sub>

Arpan Paikar,  Phong Thai,  Matthew T. Figgins,  Bodhisattwa Mandal,  Matthew J. Leka,  Joseph H. Reibenspies,  Gerard P. Van Trieste  and David C. Powers \*

Metal–imidogen (*i.e.*, M–NH) intermediates are proposed in metal-catalyzed NH-transfer reactions. Transition metal complexes of hydrazoic acid (HN<sub>3</sub>) could serve as precursors to these transient intermediates; however, the coordination chemistry of HN<sub>3</sub> is essentially unknown. Here, we report the synthesis and characterization of Rh<sub>2</sub>(esp)<sub>2</sub>(HN<sub>3</sub>)<sub>2</sub>, the first crystalline transition metal complex of HN<sub>3</sub> (esp =  $\alpha,\alpha,\alpha',\alpha'$ -tetramethyl-1,3-benzenedipropionate). Temperature-dependent multi-nuclear NMR, UV-vis, and IR spectroscopies demonstrate that HN<sub>3</sub> is a weakly coordinating ligand ( $K_{\text{eq}} = 1100 \pm 100 \text{ M}^{-2}$  at 243 K). Cryogenic photolysis (77 K) enabled observation of a non-steady state intermediate, which we assign to be a triplet Rh<sub>2</sub>–NH complex, that engages in olefin aziridination chemistry. The nitrene photochemistry of Rh<sub>2</sub>(esp)<sub>2</sub>(HN<sub>3</sub>)<sub>2</sub> was corroborated by *in crystallo* synthesis and cryogenic spectroscopic characterization of a family of *N*-aryl nitrene complexes. Together, these results establish the coordination chemistry of HN<sub>3</sub>, confirm the triplet ground state of the Rh<sub>2</sub>–NH intermediate responsible for NH transfer, and demonstrate a photochemical platform to observe intermediates in NH-transfer catalysis.

Received 18th March 2026  
Accepted 27th April 2026

DOI: 10.1039/d6sc02258h  
rsc.li/chemical-science

## Introduction

Imidogen (*i.e.*, NH) is the simplest nitrene and cryogenic matrix isolation has established its triplet ground state (*i.e.*, <sup>3</sup>[NH]).<sup>1–4</sup> Conceptually, imidogen transfer to C–H bonds and olefins would streamline access to primary amines and N–H aziridines, respectively.<sup>5–9</sup> In the absence of a catalyst, NH transfer is rarely observed: even at low temperature (~20 K), imidogen dimerizes to generate N<sub>2</sub>H<sub>2</sub> (ref. 10 and 11) and reacts unselectively with olefinic substrates to yield mixtures of HCN, N<sub>2</sub>, and alkyl nitriles (Fig. 1a).<sup>12,13</sup> Significant progress has been made towards the development of Rh<sub>2</sub>,<sup>14,15</sup> Co,<sup>16</sup> and Fe-catalyzed<sup>5,17,18</sup> NH-transfer reactions, although at present, optimization of these reactions is empirically guided because the putative M–NH intermediates have eluded experimental observation.

Hydrazoic acid (HN<sub>3</sub>)—the simplest molecular azide—is an explosive, toxic, and volatile liquid (b.p. = 310 K (37 °C)).<sup>19</sup> HN<sub>3</sub> is monomeric in the gas phase<sup>10,20–23</sup> and displays a tetrameric structure in the solid state that persists up to its melting point (190(5) K).<sup>24,25</sup> HN<sub>3</sub> can serve as a precursor to imidogen *via* photochemical N<sub>2</sub> extrusion.<sup>22,26–28</sup> Application of HN<sub>3</sub> photochemistry to the preparation of reactive M–NH complexes is currently stymied by the lack of HN<sub>3</sub> coordination chemistry. In

1970, Schmidt suggested that reaction of HN<sub>3</sub> with SbCl<sub>5</sub>—which ultimately affords NH<sub>4</sub>SbCl<sub>6</sub>, [SbCl<sub>4</sub>(N<sub>3</sub>)<sub>2</sub>], and N<sub>2</sub>—proceeds through an unobserved HN<sub>3</sub>·SbCl<sub>5</sub> adduct.<sup>29</sup> Oxidative addition of HN<sub>3</sub> with vanadium, chromium, and digermanium complexes have been observed and suggested to proceed *via* unobserved HN<sub>3</sub> adducts.<sup>30–32</sup> In 2019, Schulz reported the first—and thus far only—example of a crystalline HN<sub>3</sub> coordination compound, HN<sub>3</sub>·B(C<sub>6</sub>F<sub>5</sub>)<sub>3</sub> (Fig. 2a).<sup>33</sup> Above 253 K (–20 °C), N<sub>2</sub> loss is facile and results in aminoborane formation. The

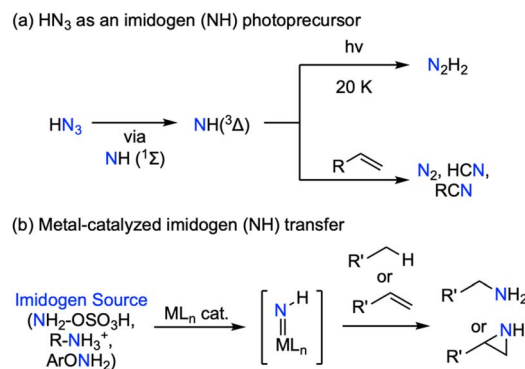


Fig. 1 (a) Photochemical synthesis of <sup>3</sup>[NH] from HN<sub>3</sub>. <sup>3</sup>[NH] dimerizes to generate N<sub>2</sub>H<sub>2</sub> and reacts with olefins to afford mixtures of nitrogen-containing products. (b) Metal-catalyzed imidogen-transfer reactions have been developed for both C–H amination and olefin aziridination.



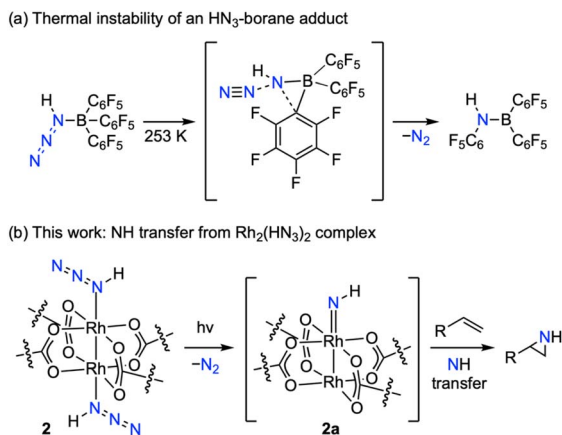


Fig. 2 (a)  $\text{HN}_3 \cdot \text{B}(\text{C}_6\text{F}_5)_3$ , the only previously reported crystalline  $\text{HN}_3$  adduct, rearranges above 253 K. (b) Here, we report the synthesis, characterization, and imidogen-transfer photochemistry of  $\text{Rh}_2(\text{esp})_2(\text{HN}_3)_2$  (**2**), the first crystalline transition metal complex of  $\text{HN}_3$ .

complete lack of transition metal complexes of  $\text{HN}_3$  prevents experimental evaluation of potential imidogen transfer chemistry from these platforms.

$\text{Rh}_2(\text{esp})_2$  (**1**) catalyzes NH-transfer from hydroxylamine derivatives to olefinic substrates and  $\text{Rh}_2(\text{II,II})\text{-NH}$  intermediates have been proposed.<sup>14,15</sup> Computational studies have suggested the proposed  $\text{Rh}_2(\text{II,II})\text{-NH}$  adopts a triplet ground state.<sup>34,35</sup>  $\text{Rh}_2(\text{II,III})$  intermediates have been suggested as alternative intermediates,<sup>36–38</sup> in part based on the facility of one-electron hydroxylamine redox chemistry.<sup>39</sup> To investigate the putative  $\text{Rh}_2$ -imidogen intermediates and establish photochemical access to  $\text{M-NH}$  species, here, we report the synthesis and characterization of the first crystalline transition metal complex of hydrazoic acid,  $\text{Rh}_2(\text{esp})_2(\text{HN}_3)_2$  (**2**) (Fig. 2b). Complex **2** is prepared by treatment of **1** with  $\text{HN}_3$  and is characterized by single-crystal X-ray diffraction (SCXRD),  $^1\text{H}$ ,  $^{13}\text{C}$ , and  $^{15}\text{N}$  NMR, IR, and UV-vis spectroscopies. Photolysis of **2** in the presence of olefinic substrates promotes stereospecific NH transfer and cryogenic photolysis suggests the intermediacy of a transient triplet  $\text{Rh}_2$  imidogen adduct (*i.e.*,  $^3[\text{Rh}_2\text{-NH}]$ ). The obtained spectroscopic data were further corroborated by *in crystallo* synthesis and spectroscopic characterization of a family of  $\text{Rh}_2$  *N*-aryl nitrene complexes. These findings indicate the chemical and kinetic competence of  $^3[\text{Rh}_2\text{-NH}]$  intermediates in NH-transfer catalysis, detail the first spectroscopic characterization of  $\text{Rh}_2$  nitrenes, and introduce new opportunities in the synthesis of reactive  $\text{M-NH}$  intermediates.

## Results and discussion

### Synthesis and characterization

$\text{Rh}_2(\text{esp})_2(\text{HN}_3)_2$  (**2**).  $\text{HN}_3$  was prepared by the addition of stearic acid to solid  $\text{NaN}_3$  (**SAFETY**:  $\text{HN}_3$  is an explosive, toxic, and volatile substance; see Fig. S1 and S2 for detailed synthetic protocol).<sup>24,25</sup> Vacuum transfer of  $\text{HN}_3$  to a  $\text{CH}_2\text{Cl}_2$  solution of **1** resulted in a color change from light green to dark green. Diffraction-quality crystals of **2** were obtained by cooling this

reaction solution to  $-20^\circ\text{C}$ . Refinement of the resulting SCXRD data revealed an  $\text{N}_\alpha$ -coordination of  $\text{HN}_3$  to both apical sites of  $\text{Rh}_2(\text{esp})_2$  (Fig. 3a). The  $\text{Rh}(1)\text{-Rh}(2)$  bond distance for **2** is  $2.382(1)$  Å (*c.f.*, for **1**,  $\text{Rh-Rh}$  is  $2.3817(9)^{40}$ ) and the  $\text{Rh}(1)\text{-N}(1)$  distance is  $2.317(2)$  Å, which is similar to previously reported aryl and alkyl azide complexes of  $\text{Rh}_2$ .<sup>41,42</sup> The  $\text{N-N-N}$  bond angle ( $172.2(3)^\circ$ ) and the  $\text{N}(1)\text{-N}(2)$  and  $\text{N}(2)\text{-N}(3)$  bond lengths ( $1.246(3)$  and  $1.122(3)$  Å, respectively) of **2** are similar to those of  $(\text{HN}_3)_4$ .<sup>33</sup>

The solid-state IR spectrum of **2** (ATR) features a broad N-H peak at  $3212\text{ cm}^{-1}$  and two peaks at  $2143\text{ cm}^{-1}$  and  $1176\text{ cm}^{-1}$  corresponding to the asymmetric and symmetric azide stretches, respectively (Fig. 3b). For comparison, we also prepared  $^2\text{H}$ - and  $^{15}\text{N}$ -labeled **2** (*i.e.*,  $[\text{H}^2]\text{-2}$  and  $[\text{N}^{15}]\text{-2}$ ) by vacuum transfer of  $\text{DN}_3$  and  $\text{H}^{15}\text{NN}_2$ , respectively.  $[\text{N}^{15}]\text{-2}$  displays solid-state IR features that are slightly red-shifted compared to **2** at  $3196\text{ cm}^{-1}$ ,  $2119\text{ cm}^{-1}$ , and  $1166\text{ cm}^{-1}$  (Fig. 3b).  $[\text{H}^2]\text{-2}$  displays an N-D stretch at  $2388\text{ cm}^{-1}$  (compared with an N-H stretch at  $3112\text{ cm}^{-1}$  for **2**) and no significant perturbation of the azide stretching modes.

The  $^1\text{H}$  NMR spectrum of **2** displays diamagnetically shifted peaks that integrate as expected for **2** : **1** coordination of  $\text{HN}_3$  to **1**. The N-H chemical shift of **2** is temperature and concentration dependent (*vide infra*), but in general is sharper and shifted downfield compared to  $\text{HN}_3$  (Fig. 3c). For example, the N-H resonance of **2** is at 4.95 ppm (FWHM = 23.9 Hz) in  $\text{CD}_2\text{Cl}_2$  at 298 K; the N-H resonance of  $\text{HN}_3$  is at 4.52 ppm (FWHM = 61.1 Hz). The N-H resonance is also solvent dependent: the N-H chemical shift of **2** is at 4.95 ppm in  $\text{CD}_2\text{Cl}_2$ , 3.6 ppm in toluene-*d*<sub>8</sub> (Fig. S3), and 3.2 ppm in the solid state (measured *via* magic angle spinning (MAS) solid-state (SS)  $[\text{H}^2]\text{-NMR}$  of  $[\text{H}^2]\text{-2}$  (Fig. S4)). Finally, the  $^1\text{H}$  spectrum of  $[\text{N}^{15}]\text{-2}$  displays a doublet for the N-H peak ( $J_{\text{N-H}} = 69.0$  Hz) (Fig. 3c). The  $^1\text{H}$ -coupled  $^{15}\text{N}$  NMR spectrum of  $[\text{N}^{15}]\text{-2}$  displays two peaks: a singlet at  $-171.2$  ppm and a doublet at  $-325.2$  ppm ( $J_{\text{H-N}} = 69.7$  Hz), which we assign as  $\gamma\text{-N}$  and  $\alpha\text{-N}$ , respectively (Fig. 3d). The MAS-SS  $[\text{N}^{15}]\text{-NMR}$  of  $[\text{N}^{15}]\text{-2}$  displays analogous features at  $-159.1$  and  $-336.7$  ppm (Fig. S5).

$\text{Rh}_2(\text{esp})_2(\text{ArN}_3)_2$  (**3**). Treatment of complex **1** with  $\text{PhN}_3$ , 4-Me- $\text{C}_6\text{H}_4\text{-N}_3$ , and 4- $\text{CF}_3\text{-C}_6\text{H}_4\text{-N}_3$  afforded aryl azide complexes **3a-c**. Dark green diffraction-quality crystals of **3a-c** were obtained by layering  $\text{CH}_2\text{Cl}_2$  or  $\text{CHCl}_3$  solutions with pentane at  $-20^\circ\text{C}$ . Complexes **3** are structurally analogous to **2**: SCXRD analysis for all three compounds shows  $\text{N}_\alpha$ -coordination of  $\text{ArN}_3$  to the axial sites of  $\text{Rh}_2(\text{esp})_2$  (**1**) (Fig. 4). The  $\text{Rh}(1)\text{-N}(1)$  bond distances of **3a-c** are  $2.261(2)$  Å,  $2.300(2)$  Å, and  $2.271(3)$  Å (avg.) (there are two molecules of **3c** in the asymmetric unit), respectively, and  $\sim 0.1$  Å shorter than the  $\text{Rh}(1)\text{-N}(1)$  bond of **2**.  $^1\text{H}$  NMR data of **3a-c** confirms **2** : **1** coordination of the aryl azide ligands to **1**; during solvent removal from **3c**, partial loss of the apical azides was evident by integration of the  $^1\text{H}$  NMR spectrum. The solid-state IR spectra display azide stretches at  $\sim 2100$  and  $\sim 2130\text{ cm}^{-1}$  for **3a-3c** (Fig. S6).<sup>43</sup>



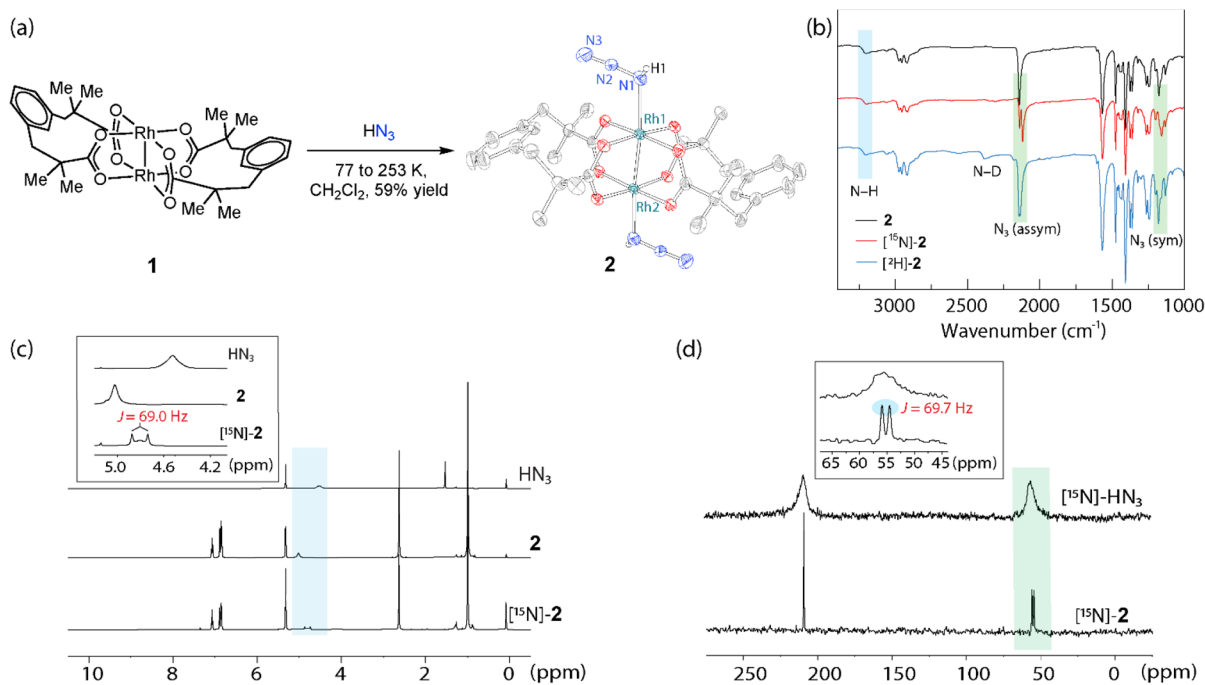


**Fig. 3** (a) Treatment of  $\text{Rh}_2(\text{esp})_2$  (**1**) with  $\text{HN}_3$  affords  $\text{Rh}_2(\text{esp})_2(\text{HN}_3)_2$  (**2**). Displacement ellipsoid plot of **2** plotted at 50% probability; data were collected at 100 K. H-Atoms, except H1, and  $\text{CH}_2\text{Cl}_2$  are removed for clarity. Selected metrics:  $\text{Rh}(1)-\text{Rh}(2)$ : 2.382(1) Å,  $\text{Rh}(1)-\text{N}(1)$ : 2.317(2) Å,  $\text{N}(1)-\text{N}(2)$ : 1.246(3) Å,  $\text{N}(2)-\text{N}(3)$ : 1.122(3) Å,  $\text{N}(1)-\text{N}(2)-\text{N}(3)$ : 172.2(3)°. (b) Solid-state IR spectra of **2** (black trace),  $^{15}\text{N}$ -**2** (red trace), and  $^2\text{H}$ -**2** (blue trace) plotted from 3500  $\text{cm}^{-1}$  to 1000  $\text{cm}^{-1}$ . The blue shaded area highlights peak shift of the N–H stretch, and the green shaded area compares azide stretches for compounds **2**,  $^{15}\text{N}$ -**2**, and  $^2\text{H}$ -**2**. (c)  $^1\text{H}$  NMR spectra of  $\text{HN}_3$ , **2**, and  $^{15}\text{N}$ -**2**; the concentration-dependent N–H resonances are highlighted in blue. Inset: Expansion highlighting the N–H resonances. (d) Proton-coupled  $^{15}\text{N}$  NMR spectra of  $^{15}\text{N}$ - $\text{HN}_3$  and  $^{15}\text{N}$ -**2**; the  $^{15}\text{N}$  resonances attributable to the N–H are highlighted in green. Inset: Peak splitting for  $^{15}\text{N}$ -**2** due to the  $^{15}\text{N}$ – $^1\text{H}$  coupling ( $J = 69.7$  Hz).

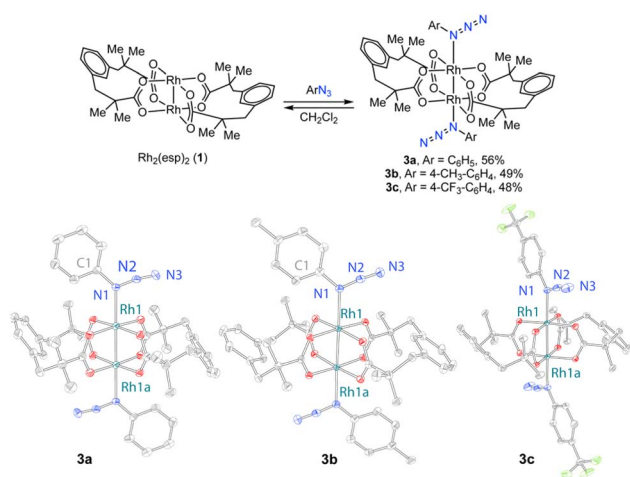


**Fig. 4** Synthesis and characterization of dirhodium aryl azide compounds **3**. Solid-state structure of compounds **3a–c**. Displacement ellipsoid plots of **3a–c** plotted at 50% probability; data were collected at 100 K. H-Atoms and solvents of crystallization are removed for clarity. Selected metrics:  $\text{Rh}(1)-\text{N}(1)$ : 2.261(2) Å for **3a**, 2.301(2) Å for **3b**, and 2.271(3) Å (avg.) for **3c**.

### Ligand binding thermodynamics

The  $\text{HN}_3$  ligands of **2** are labile in solution. The N–H chemical shift in the  $^1\text{H}$  NMR of **2** is temperature (and concentration)

dependent and shifts downfield upon cooling from 298 K to 203 K (Fig. 5a). Similar temperature dependence is reflected in VT- $^{15}\text{N}$  NMR experiments (Fig. S7). VT-IR spectroscopy similarly indicates facile equilibration of **2** and **1** +  $\text{HN}_3$  (Fig. 5b): a  $\text{CH}_2\text{Cl}_2$  solution of **2** displays two azide stretching frequencies at 273 K—at 2138 and 2151  $\text{cm}^{-1}$ —which we assign to  $\text{HN}_3$  and **2**, respectively (in the solid-state the azide stretches for **2** appears at 2143  $\text{cm}^{-1}$ ).<sup>44,45</sup> Upon cooling, the relative intensity of these spectral features changes, with the free  $\text{HN}_3$  stretch decreasing in intensity while the coordinated  $\text{HN}_3$  stretch increases in intensity. Similar temperature dependence is noted in analysis of the symmetric vibrational mode and in VT-UV-vis measurements (Fig. S8 and S9).

To evaluate the thermodynamics of  $\text{HN}_3$  binding, we carried out an NMR titration of  $\text{HN}_3$  with **1** at 243 K ( $-30$  °C). The N–H resonance of  $\text{HN}_3$  is systematically shifted downfield with increasing  $[\mathbf{1}]$  (Fig. S10). Using equations derived analogously to those of Drago,<sup>46</sup> these data enabled determination of temperature-dependent equilibrium constants ( $K_{\text{eq}}$ ):  $K_{\text{eq}} = 1100 \pm 100 \text{ M}^{-2}$  at 243 K;  $K_{\text{eq}} = 120 \text{ M}^{-2}$  at 298 K. Van't Hoff analysis (Fig. S11), based on the obtained temperature-dependent equilibrium constants, provided  $\Delta H^0 = -5.5 \pm 0.1 \text{ kcal mol}^{-1}$  and  $\Delta S^0 = -9.0 \pm 0.6 \text{ cal K}^{-1} \text{ mol}^{-1}$ . The  $K_{\text{eq}}$  for  $\text{HN}_3$  binding is similar to that determined by Albrecht for the coordination of  $\text{AdN}_3$  to  $\text{Fe}(\text{HMDS})_2$  ( $62 \text{ M}^{-1}$  at 298 K) ( $\text{Ad} = \text{adamantyl}$ ).<sup>44</sup>



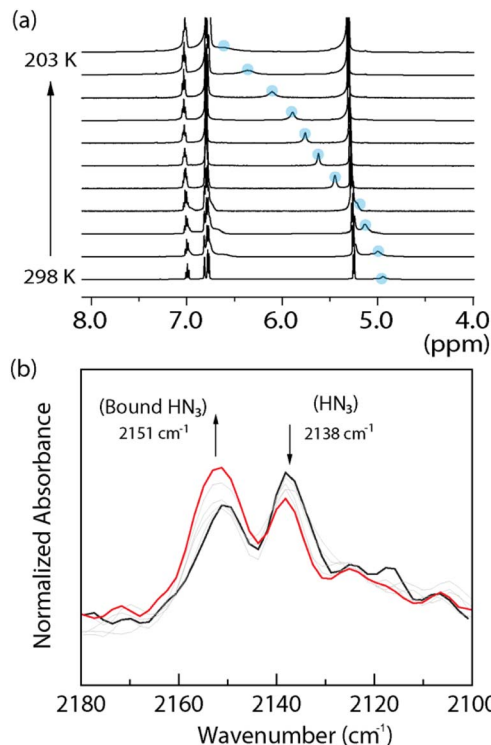


Fig. 5 (a) VT- $^1\text{H}$  NMR spectra of **2** collected in  $\text{CD}_2\text{Cl}_2$  from 298 K to 203 K. The N-H resonance is highlighted in blue. (b) Solution-phase VT-IR spectra of **2** collected in  $\text{CD}_2\text{Cl}_2$  from 273 K (black) to 233 K (red).

We similarly carried out an NMR titration of  $\text{PhN}_3$  with **1** (Fig. S12) to evaluate the thermodynamics of aryl azide binding. The obtained data provided  $K_{\text{eq}} = 11\,000 \pm 3000 \text{ M}^{-2}$  at 243 K ( $K_{\text{eq}} = 2700 \text{ M}^{-2}$  at 298 K), which is slightly larger than that measured for  $\text{HN}_3$  (for VT-NMR of compound **3a**, see Fig. S13). The relative binding affinities are consistent with enhanced Lewis basicity of  $\text{Ph-N-N}_2$  as compared with  $\text{H-N-N}_2$ .<sup>47</sup> Van't Hoff analysis, based on  $K_{\text{eq}}$  measurements from 298 K to 203 K provided  $\Delta H^0 = -4.23 \pm 0.06 \text{ kcal mol}^{-1}$  and  $\Delta S^0 = 1.5 \pm 0.2 \text{ cal K}^{-1} \text{ mol}^{-1}$  (Fig. S14). Temperature-dependent UV-vis spectroscopic data of **3a-c** are collected in Fig. S15. In comparison to common nitrogen donors, such as pyridine and acetonitrile ( $K_{\text{eq}} > 10^3$  for binding to  $\text{Rh}_2$ ),  $\text{HN}_3$  and aryl azides are weakly binding ligands.<sup>48-51</sup>

### NH-transfer photochemistry

To chemically evaluate the competence of photochemically generated intermediates to engage in N-H transfer, we pursued the study of the NH-transfer photochemistry of **2** with olefinic substrates. Photolysis ( $\lambda = 300 \text{ nm}$ , 243 K, quartz reaction vessel) of a  $\text{CD}_2\text{Cl}_2$  solution of **2** in the presence of 1-octene resulted in NH transfer to afford the corresponding N-H aziridine (**4**) in 39% yield (Fig. 6); compound **1** is observed as the Rh-containing byproduct by  $^1\text{H}$  NMR (for  $^1\text{H}$  and ESI-MS analysis see Fig. S16 and S17). Similarly, photolysis of  $^{15}\text{N}$ -**2** in the presence of 1-octene affords a 1 : 1 mixture of **4** :  $^{15}\text{N}$ -**4**, which is expected from a mono-labeled  $^{15}\text{N}$ - $\text{HN}_3$  precursor (Fig. S18

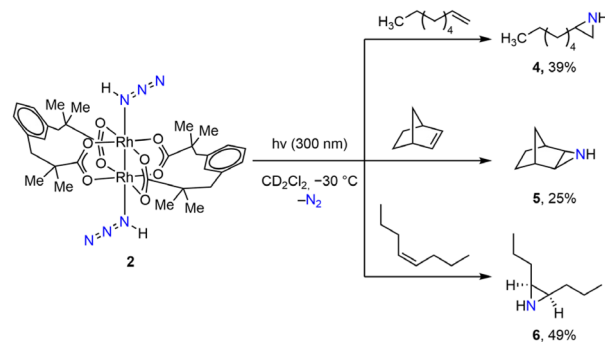


Fig. 6 N-H transfer photochemistry of **2** with olefins. Photochemical olefin aziridination by **2** is stereospecific. Yields obtained by  $^1\text{H}$  NMR spectroscopy.

and S19). In this experiment,  $^{15}\text{N}$ - $\text{N}_2$  was also observed by  $^{15}\text{N}$ -NMR ( $-70.3 \text{ ppm}$ ),<sup>52</sup> which demonstrates the facility of  $\text{N}_2$  photoelimination under these reaction conditions (Fig. S20). NH transfer to 1-octene was also observed for photolysis of a toluene solution, albeit in lower yield (12%), which we attribute to limited solubility of **2** at low temperature in this solvent (Fig. S21). For comparison, photolysis of a  $\text{CD}_2\text{Cl}_2$  solution of  $\text{HN}_3$  and 1-octene in the absence of **1** did not give rise to any observable NH-transfer products (Fig. S22).

Photolysis of **2** in the presence of norbornene affords the corresponding N-H aziridine **5** in 25% yield (for  $^1\text{H}$  and ESI-MS analysis see Fig. S23 and S24).<sup>53</sup> Photochemically promoted N-H transfer is stereospecific: photolysis of **2** in the presence of *cis*-4-octene afforded *cis*-**6** exclusively (49% yield) (for  $^1\text{H}$  and ESI-MS analysis see Fig. S25 and S26). This observation is consistent with the stereospecific NH transfer that has been noted in  $\text{Rh}_2$ -catalyzed imidogen-transfer reactions.<sup>14,15</sup> The modest yields of aziridines in these reactions are likely due to competing reaction of free NH with olefins: *N*-chloromethylamine was also observed as reaction byproducts (Fig. S27-S29).<sup>13,54,55</sup>

In contrast to the observed NH-transfer photochemistry from **2**, photolysis of **3a-c** in the presence of 1-octene did not result in nitrene transfer products (*i.e.*, *N*-aryl aziridines or allylic amination products). This observation is consistent with facile intramolecular rearrangement of aryl nitrenes.<sup>56</sup>

Together, the results of these NH-transfer experiments indicate that the photogenerated intermediate from **2** is chemically and kinetically competent as an intermediate in the  $\text{Rh}_2$ -catalyzed NH-transfer.

### Observation of reactive nitrenes

**Cryogenic photolysis of 2.** Given the observation of imidogen transfer photochemistry from **2**, we sought to observe the putative  $\text{Rh}_2$ -NH intermediate (*i.e.*, **7**, Fig. 7a). To this end, we carried out photolysis of a 2,2-dimethylbutane (DMB):*tert*-butylbenzene (TBB) (3 : 1) glass of **2** at 77 K in a quartz J-Young EPR tube. This solvent system was chosen to provide an optical glass while avoiding ligand exchange with more common glassy solvents such as 2-methyltetrahydrofuran.<sup>57</sup> Photolysis of **2** at 77 K results in a small but reproducible blue shift of the



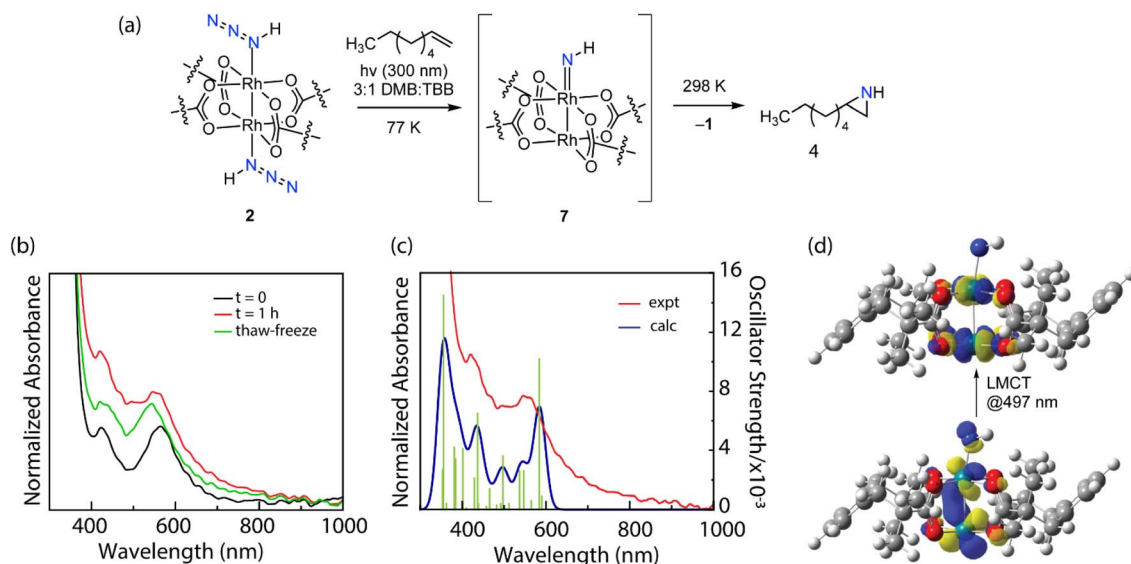


Fig. 7 (a) Cryogenic photolysis ( $\lambda = 300$  nm) of complex 2. (b) UV-vis spectra of 2 (black), 7 (i.e., after 1 h photolysis, red), and after thermal annealing (green) collected at 77 K. (c) UV-vis spectrum of 7 at 77 K (red) overlaid with the simulated spectrum of compound 7 (blue) based on the  $^3$ TD- $^3$ DFT calculation by PBE0-D3-BS1 method. Vertical transition pictured in green. (d) Principal NTOs for the transition at 497 nm.

absorbance centered at 570 nm to 560 nm and the concurrent growth of significant spectral intensity  $\sim 500$  nm (Fig. 7b). These spectral features arise from a non-steady state intermediate: thermal annealing of the sample to 298 K followed by re-freezing at 77 K results in the disappearance of the spectral intensity at 500 nm and the growth of a new absorbance centered at 543 nm, which overlays the spectrum of  $\text{Rh}_2(\text{esp})_2$  (1) in this solvent mixture (Fig. S30 and S31). We carried out analogous cryogenic photolysis of  $^{15}\text{N}$ -2 in a 3 : 1 DMB : TBB glass with the addition of 1-octene. Spectra obtained during this photolysis indicated the formation of the same non-steady state intermediate observed in the absence of 1-octene (Fig. S32). Thermal annealing of this sample led to disappearance of the non-steady state intermediate and the evolution of a 1 : 1 mixture of 4 and  $^{15}\text{N}$ -4, which demonstrates NH-transfer reactivity from the observed non-steady state intermediate (Fig. S33).

We assign the non-steady state intermediate observed during 77 K photolysis to  $\text{Rh}_2\text{-NH}$  complex  $^3[7]$ . The spectral features observed after cryogenic photolysis of 2 are consistent with TD-DFT calculations of  $^3[7]$  (Fig. 7c).<sup>58</sup> DFT single points of the singlet and triplet imidogen complexes (i.e.  $^1[7]$  and  $^3[7]$  at the SMD-PBE0-D3/Def2-TZVP level of theory) were used to calculate the  $\Delta E_{\text{ST}}$  ( $\Delta E_{\text{ST}} = E_{\text{Singlet}} - E_{\text{Triplet}}$ ) to be 11.9 kcal mol $^{-1}$ . To further confirm this, single points at the DLPNO-CCSD(T)/Def2-TZVP level of theory were run and provided a  $\Delta E_{\text{ST}}$  of 15.2 kcal mol $^{-1}$ . The TD-DFT calculations of 2 and  $^3[7]$ , using *tert*-butylbenzene as an implicit solvent model, suggest that conversion of 2 to  $^3[7]$  should be accompanied by minor changes in the absorbances at  $\sim 570$  and  $\sim 425$  nm but also the emergence of a new LMCT transition at 497 nm (Fig. 7d).<sup>59</sup> This computed transition is well-matched to the growth of intensity observed experimentally at 500 nm (Fig. S34). In contrast, the observed spectral features are not well-matched to the

computed spectrum of  $^1[7]$  (Fig. S35). Further, the observed spectral features are inconsistent with the formation of  $\text{Rh}_2(\text{-II,III})$ , which typically display low energy UV-vis transitions.<sup>35,36</sup>

Formulation as  $^3[7]$  is consistent with the metrical parameters that we previously reported for triplet adamantyl and biaryl nitrenes of  $\text{Rh}_2$  obtained by *in crystallo* photochemistry.<sup>40,60-62</sup> Attempts to accomplish *in crystallo* synthesis of 7 were not productive due to loss of crystallinity during sample photolysis.

**Cryogenic photolysis of 3a-3c.** Guided by the hypothesis that *N*-arylation would provide a handle to modulate the electronic absorption spectra of the resulting nitrene, we carried out the cryogenic photolysis of aryl azide complexes 3a-3c (Fig. 8a and b). Photolysis of 3a in a 3 : 1 DMB : TBB glass at 77 K gave rise to a new absorption features centered at 510 nm and 620 nm. Thermal annealing led to the disappearance of these spectroscopic features. Similar to 7, the experimental UV-vis spectra of 8a was qualitatively similar to the TD-DFT simulated spectrum computed for a triplet nitrene although the simulated spectrum is blue-shifted as compared to experiment (for full spectral evolution see Fig. S36). TD-DFT calculations of  $^3[8a]$  show transitions with moderate oscillator strength ( $>0.01$ ) at 469 nm and 516 nm (Fig. S37a). Comparison of the simulated spectral shape and relative oscillator strengths suggests the transition at 469 nm corresponds to the sharper experimental feature at 510 nm whereas the transition at 516 nm corresponds to the feature at 620 nm. Natural Transition Orbital (NTO) analysis shows that the higher energy transition is MLCT from a Rh  $\beta$  d orbital into the SUMO that is delocalized between the nitrene N p orbital and the aryl group and the lower energy transition at 516 nm is mostly comprised of a Rh  $\alpha$  d-to-d transition (Fig. 8c, for all the NTOs of  $^3[8a]$ , see Fig. S37b).

Cryogenic photolysis of 3b also resulted in the evolution of a non-steady state intermediate (for full spectral evolution see Fig. S38). The spectral features of  $^3[8b]$  were observed at 507 nm



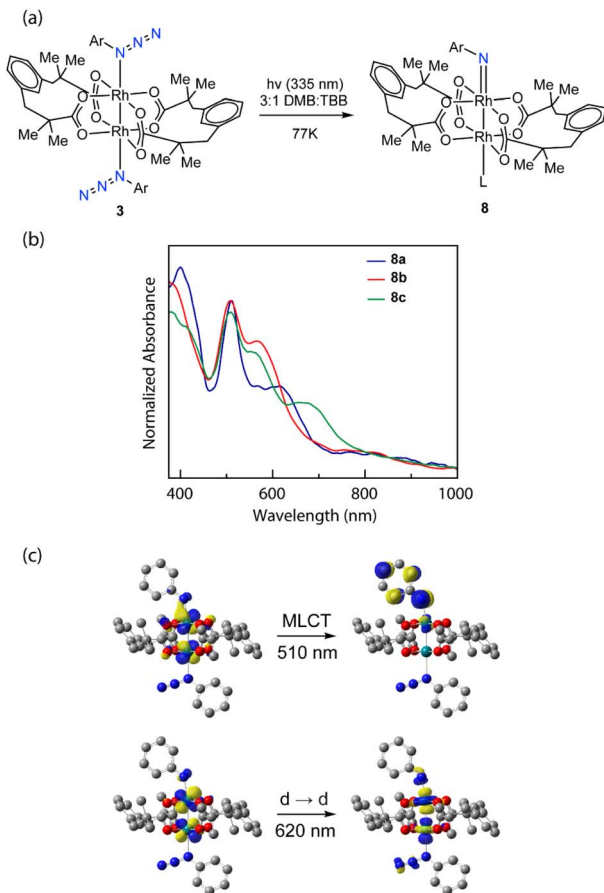


Fig. 8 (a) Photolysis ( $\lambda = 335$  nm) of complexes **3** at 77 K generates *N*-aryl nitrenes **8**. (b) UV-vis spectra of **8a** (red), **8b** (blue), and **8c** (green) collected at 77 K. (c) Principal NTOs for the transitions at 510 nm and 620 nm of  $^3[\mathbf{8a}]$ .

and 571 nm and TD-DFT calculations result in a simulated spectrum (Fig. S39a) that qualitatively aligns with experiment much like in the case of  $^3[\mathbf{8a}]$  and shows a blue shift for the higher energy peak relative to  $^3[\mathbf{8a}]$  (463 nm for  $^3[\mathbf{8b}]$  and 469 nm for  $^3[\mathbf{8a}]$ ). NTO analysis indicates the parentage of these transitions is similar to that of the features observed for  $^3[\mathbf{8a}]$  (Fig. S39b). The observed blue-shift of the peaks is consistent with methylation raising the energy of the acceptor orbital for the observed transitions. Superficially, the results obtained from cryogenic photolysis of **3c** also indicate the formation of a non-steady state intermediate (for full spectral evolution, see Fig. S40). In this case however, evacuation of the solvent during the preparation of the glassy solvent matrix resulted in partial loss of the azide ligand (*vide supra*) and thus quantitative comparisons of the resulting optical spectrum are not possible (for TD-DFT and NTO analysis of  $^3[\mathbf{8c}]$ , see Fig. S41).

*In crystallo* photolysis of **3** provided experimental metrical parameters for the corresponding  $\text{Rh}_2$  nitrenes (*i.e.*,  $^3[\mathbf{8a}]$ ,  $^3[\mathbf{8b}]$ , and  $^3[\mathbf{8c}]$ ) and confirmed the nitrene chemistry implied by the aforementioned spectroscopic and computational studies (Fig. 9, for  $^3[\mathbf{8a}]$ , and  $^3[\mathbf{8c}]$ , see Fig. S42 and S43, respectively). Photolysis of single crystals of **3** resulted in 30–50%

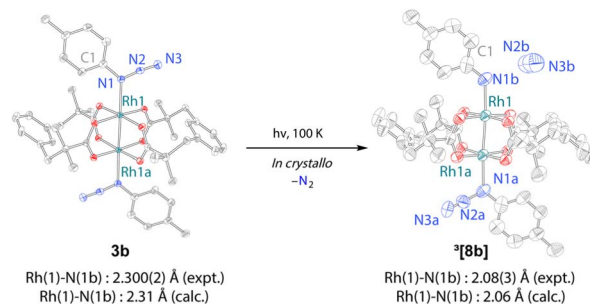


Fig. 9 *In crystallo* characterization of  $^3[\mathbf{8b}]$ , upon photo-extrusion of  $\text{N}_2$  molecule from **3b** with 35% photoconversion. The obtained metrical parameters are well-matched to the optimized geometry for triplet *N*-aryl nitrene (*i.e.*,  $^3[\mathbf{8b}]$ ).

photoconversion to the corresponding nitrenes before loss of crystallinity. In all cases,  $\text{N}_2$  loss was associated with shortening of both the  $\text{Rh}(1)\text{--N}(1)$  bonds (*i.e.*,  $\sim 0.3$  Å for  $\text{Rh}(1)\text{--N}(1)$ ). Though we cannot locate the  $\text{N}_2$  molecule *in crystallo* for **8a** and **8c** due to disorder, for **8b**, *in crystallo* photoextrusion of  $\text{N}_2$  from **3b** was observed. The metrical parameters of **8a**, **8b**, and **8c** are consistent with formulation as triplet complexes. DFT single points at the SMD-PBE0-D3/Def2-TZVP level of theory were used to calculate the  $\Delta E_{\text{ST}}$  to be 11.4 kcal mol $^{-1}$ , 9.1 kcal mol $^{-1}$ , and 12.4 kcal mol $^{-1}$  for  $^3[\mathbf{8a}]$ ,  $^3[\mathbf{8b}]$ , and  $^3[\mathbf{8c}]$ , respectively.

## Conclusions

Here, we describe the first structurally characterized transition metal complex of hydrazoic acid,  $\text{Rh}_2(\text{esp})_2(\text{HN}_3)_2$  (**2**), by addition of gaseous  $\text{HN}_3$  to  $\text{Rh}_2(\text{esp})_2$  (**1**). Temperature-dependent NMR, UV-vis, and IR measurements indicate that the  $\text{HN}_3$  ligands are labile in solution;  $K_{\text{eq}} = 1100 \pm 100 \text{ M}^{-2}$  at 243 K. Complex **2** engages in stereospecific NH-transfer photochemistry with olefins, which suggests that the same intermediate is accessed during photolysis of **2** as is generated during  $\text{Rh}_2$ -catalyzed NH-transfer reactions.<sup>9</sup> Cryogenic photolysis of **2** in a frozen solvent glass enabled observation of the transient  $\text{Rh}_2\text{--NH}$  intermediate. Comparison of the spectroscopic data with results of DFT and TD-DFT calculations suggest this intermediate displays a triplet ground state (*i.e.*,  $^3[7]$ ).

Analogous aryl azide complexes provided further support for the structural and spectroscopic assignments in the hydrazoic acid photochemistry. Cryogenic UV-vis spectroscopy provided evidence for the intermediacy of  $^3[\text{Rh}_2\text{--NAr}]$  complexes and bolstered the computationally supported spectroscopic assignments for  $^3[\text{Rh}_2\text{--NH}]$ . In addition, *in crystallo* synthesis provided experimental definition of the metrical parameters of the aryl nitrene adducts, which both confirms the nitrene photochemistry of this family of azide complexes as well as further supports the formulation as triplet adducts. Together, these results introduce  $\text{HN}_3$  as a ligand in transition metal coordination chemistry, enable photochemical generation of  $\text{M}\text{--NH}$  species, and provide new tools to study metal-catalyzed amination chemistry.



## Author contributions

A. P., G. P. V. T., and D. C. P. conceptualized the project. A. P., P. T., M. T. F., B. M., M. J. L., J. H. R., and G. P. V. T. carried out experimental work. The manuscript was written with contributions from all authors.

## Conflicts of interest

There are no conflicts to declare.

## Data availability

Experimental details and spectral data are available in the supplementary information (SI). Supplementary information: experimental procedures, spectral data, Cartesian coordinates for the calculated structures, and X-ray diffraction details. See DOI: <https://doi.org/10.1039/d6sc02258h>.

CCDC 2404479, 2514293, 2514304, 2516143, 2523419, 2523425 and 2524966 contain the supplementary crystallographic data for this paper.<sup>63a-g</sup>

## Acknowledgements

The U.S. Department of Energy (DOE), Office of Science, Office of Basic Energy Sciences, Catalysis Program (DE-SC0024121) and the Welch Foundation (A-1907) are acknowledged for funding. Texas A&M University HPRC provided computational resources (<https://hprc.tamu.edu>).

## References

- R. F. Klima and A. D. Gudmundsdóttir, *J. Photochem. Photobiol., A*, 2004, **162**, 239–247.
- N. P. Gritsan and M. S. Platz, *Chem. Rev.*, 2006, **106**, 3844–3867.
- D. Wang, W. Chen, H. Chen, Y. Chen, S. Ye and G. Tan, *Nat. Chem.*, 2024, **17**, 38–43.
- M. Janssen, T. Frederichs, M. Olaru, E. Lork, E. Hupf and J. Beckmann, *Science*, 2024, **385**, 318–321.
- Z.-J. Jia, S. Gao and F. H. Arnold, *J. Am. Chem. Soc.*, 2020, **142**, 10279–10283.
- R. R. Anugu, S. Munnuri and J. R. Falck, *J. Am. Chem. Soc.*, 2020, **142**, 5266–5271.
- A. Boullé, A. Doumbia, J.-P. Mahy and F. Avenier, *Chem. Commun.*, 2023, **59**, 79–81.
- J. L. Jat, D. Chandra, P. Kumar, V. Singh and B. Tiwari, *Synthesis*, 2022, **54**, 4513–4520.
- Y. Gelato, L. Marraffa, F. Pasca, P. Natho, G. Romanazzi, A. Tota, M. Colella and R. Luisi, *J. Am. Chem. Soc.*, 2025, **147**, 35567–35575.
- E. Amble and B. P. Dailey, *J. Chem. Phys.*, 1950, **18**, 1422.
- Dimerization of <sup>3</sup>[NH] to generate <sup>1</sup>[HN–NH] is a spin-allowed reaction according to the Carter–Goddard–Malrieu–Trinquier (CCMT) rules; see, M. Driess and H. Grützmacher, *Angew. Chem., Int. Ed.*, 1996, **35**, 828–856; P. Power, *Chem. Rev.*, 1999, **99**, 3463–3504.
- E. Jacox and D. E. Milligan, *J. Am. Chem. Soc.*, 1963, **85**, 278–282.
- D. W. Cornell, R. S. Berry and W. Lwowski, *J. Am. Chem. Soc.*, 1966, **88**, 544–550.
- Z. Ma, Z. Zhou and L. Kürti, *Angew. Chem., Int. Ed.*, 2017, **56**, 9886–9890.
- J. L. Jat, M. P. Paudyal, H. Gao, Q.-L. Xu, M. Yousufuddin, D. Devarajan, D. H. Ess, L. Kürti and J. R. Falck, *Science*, 2014, **343**, 61–65.
- W. Xue, Z. Zhu, S. Chen, B. You and C. Tang, *J. Am. Chem. Soc.*, 2023, **145**, 4142–4149.
- R. Mao, S. Gao, Z.-Y. Qin, T. Rogge, S. J. Wu, Z.-Q. Li, A. Das, K. N. Houk and F. H. Arnold, *Nat. Catal.*, 2024, **7**, 585–592.
- F.-X. Fan, H. Xu, S.-X. Tang, Y. Dang and F. Wang, *Nat. Commun.*, 2025, **16**, 1471.
- T. Curtius, *Ber. Dtsch. Chem. Ges.*, 1890, **23**, 3023–3033.
- E. H. Eyster, *J. Chem. Phys.*, 1940, **8**, 135–142.
- V. Schomaker and R. Spurr, *J. Am. Chem. Soc.*, 1942, **64**, 1184–1187.
- O. Kajimoto, T. Yamamoto and T. Fueno, *J. Phys. Chem.*, 1979, **83**, 429–435.
- J. Lievin, J. Breulet and G. Verhaegen, *Theor. Chim. Acta*, 1979, **52**, 75–88.
- J. Evers, G. Oehlinger, F. X. Steemann and T. M. Klapötke, *Inorg. Chem.*, 2020, **59**, 17671–17677.
- J. Evers, M. Göbel, B. Krumm, F. Martin, S. Medvedyev, G. Oehlinger, F. X. Steemann, I. Troyan, T. M. Klapötke and M. I. Eremets, *J. Am. Chem. Soc.*, 2011, **133**, 12100–12105.
- H.-J. Himmel, M. Junker and H. Schnöckel, *J. Chem. Phys.*, 2002, **117**, 3321–3326.
- S. L. Laursen, J. E. Grace, R. L. DeKock and S. A. Spronk, *J. Am. Chem. Soc.*, 1998, **120**, 12583–12594.
- J. N. Russell, V. M. Bermudez and A. Leming, *Langmuir*, 1996, **12**, 6492–6500.
- A. Schmidt, *Z. Anorg. Allg. Chem.*, 1971, **381**, 31–39.
- M. Morán and M. Gayoso, *J. Organomet. Chem.*, 1983, **243**, 423–426.
- H. Schäfer, W. Saak and M. Weidenbruch, *J. Organomet. Chem.*, 2000, **604**, 211–213.
- Z. D. Brown, J. D. Erickson, J. C. Fettinger and P. P. Power, *Organometallics*, 2013, **32**, 617–622.
- K. Bläsing, J. Bresien, R. Labbow, D. Michalik, A. Schulz, M. Thomas and A. Villinger, *Angew. Chem., Int. Ed.*, 2019, **58**, 6540–6544.
- R. Lorpitthaya, Z.-Z. Xie, K. B. Sophy, J.-L. Kuo and X.-W. Liu, *Chem.–Eur. J.*, 2010, **16**, 588–594.
- X. Lin, C. Zhao, C.-M. Che, Z. Ke and D. L. Phillips, *Chem.–Asian J.*, 2007, **2**, 1101–1108.
- K. P. Kornecki and J. F. Berry, *Chem.–Eur. J.*, 2011, **17**, 5827–5832.
- D. N. Zalatan and J. Du Bois, *J. Am. Chem. Soc.*, 2009, **131**, 7558–7559.
- R. H. Perry, T. J. Cahill, J. L. Roizen, J. Du Bois and R. N. Zare, *Proc. Natl. Acad. Sci. U. S. A.*, 2012, **109**, 18295–18299.
- P. Bishnoi, A. Singh, Y. Maurya, V. Jhamb, A. Sharma, S. V. Sivapreetha and S. Chatterjee, *ACS Org. Inorg. Au*, 2025, **5**, 385–399.



- 40 C. G. Espino, K. W. Fiori, M. Kim and J. Du Bois, *J. Am. Chem. Soc.*, 2004, **126**, 15378–15379.
- 41 A. Das, Y.-S. Chen, J. H. Reibenspies and D. C. Powers, *J. Am. Chem. Soc.*, 2019, **141**, 16232–16236.
- 42 A. Das, G. P. Van Trieste and D. C. Powers, *Comments Inorg. Chem.*, 2020, **40**, 116–158.
- 43 A. Das, C.-H. Wang, G. P. Van Trieste, C.-J. Sun, Y.-S. Chen, J. H. Reibenspies and D. C. Powers, *J. Am. Chem. Soc.*, 2020, **142**, 19862–19867.
- 44 W. Stroek, M. Keilwerth, L. A. Malaspina, S. Grabowsky, K. Meyer and M. Albrecht, *Chem.–Eur. J.*, 2024, **30**, e202303410.
- 45 Analogous VT-IR experiments were used to characterize the binding equilibrium of adamantyl azide (AdN<sub>3</sub>) with Fe(HMDS)<sub>2</sub>.
- 46 R. S. Drago, *Physical Methods for Chemists*, Saunders College Publishing, 1992.
- 47 E. P. L. Hunter and S. G. Lias, *J. Phys. Chem. Ref. Data*, 1998, **27**, 413–656.
- 48 R. S. Drago, S. P. Tanner, R. M. Richman and J. R. Long, *J. Am. Chem. Soc.*, 1979, **101**, 2897–2903.
- 49 R. S. Drago, J. R. Long and R. Cosmano, *Inorg. Chem.*, 1981, **20**, 2920–2927.
- 50 R. S. Drago, J. R. Long and R. Cosmano, *Inorg. Chem.*, 1982, **21**, 2196–2202.
- 51 A. F. Trindade, J. A. S. Coelho, C. A. M. Afonso, L. F. Veiros and P. M. P. Gois, *ACS Catal.*, 2012, **2**, 370–383.
- 52 K. Banert, N. Singh, B. Fiedler, J. Friedrich, M. Korb and H. Lang, *Chem.–Eur. J.*, 2015, **21**, 15092–15099.
- 53 Photopolymerization of styrenes upon UV irradiation prevented evaluation of potential N–H transfer to these substrates.
- 54 S. Kodama, *Bull. Chem. Soc. Jpn.*, 1983, **56**, 2363–2370.
- 55 Attempts to achieve photocatalysis by carrying out photolysis of solutions of **1** with excess HN<sub>3</sub> and olefinic substrates were unsuccessful, presumably due to preferential product binding to **1**.
- 56 H. Inui, K. Sawada, S. Oishi, K. Ushida and R. J. McMahon, *J. Am. Chem. Soc.*, 2013, **135**, 10246–10249.
- 57 K. S. Suslick, J. F. Bautista and R. A. Watson, *J. Am. Chem. Soc.*, 1991, **113**, 6111–6114.
- 58 <sup>3</sup>[7] is presumably generated from **2** by initial excitation to a singlet excited state that undergoes intersystem crossing to a triplet excited state from which N<sub>2</sub> dissociation proceeds.
- 59 The low energy feature at around 1100 nm was not observed as the spectrometer collection range was 100–1060 nm.
- 60 A. Paikar, G. P. Van Trieste, A. Das, C.-W. Wang, T. E. Sill, N. Bhuvanesh and D. C. Powers, *Inorg. Chem.*, 2023, **62**, 12557–12564.
- 61 Y. Baek, A. Das, S.-L. Zheng, J. H. Reibenspies, D. C. Powers and T. A. Betley, *J. Am. Chem. Soc.*, 2020, **142**, 11232–11243.
- 62 A. Sur and D. C. Powers, *ACS Cent. Sci.*, 2025, **11**, 8348–8352.
- 63 (a) CCDC 2404479: Experimental Crystal Structure Determination, 2026, DOI: [10.5517/ccdc.csd.cc2lq1v7](https://doi.org/10.5517/ccdc.csd.cc2lq1v7); (b) CCDC 2514293: Experimental Crystal Structure Determination, 2026, DOI: [10.5517/ccdc.csd.cc2qdb7q](https://doi.org/10.5517/ccdc.csd.cc2qdb7q); (c) CCDC 2514304: Experimental Crystal Structure Determination, 2026, DOI: [10.5517/ccdc.csd.cc2qdbl2](https://doi.org/10.5517/ccdc.csd.cc2qdbl2); (d) CCDC 2516143: Experimental Crystal Structure Determination, 2026, DOI: [10.5517/ccdc.csd.cc2qg7xc](https://doi.org/10.5517/ccdc.csd.cc2qg7xc); (e) CCDC 2523419: Experimental Crystal Structure Determination, 2026, DOI: [10.5517/ccdc.csd.cc2qptmw](https://doi.org/10.5517/ccdc.csd.cc2qptmw); (f) CCDC 2523425: Experimental Crystal Structure Determination, 2026, DOI: [10.5517/ccdc.csd.cc2qptt2](https://doi.org/10.5517/ccdc.csd.cc2qptt2); (g) CCDC 2524966: Experimental Crystal Structure Determination, 2026, DOI: [10.5517/ccdc.csd.cc2qrfjg](https://doi.org/10.5517/ccdc.csd.cc2qrfjg).

